Measurement of hydrogen n-α-line Stark profiles in a turbulent plasma*

Tsu-Jye A. Nee[†‡] and Hans R. Griem
Department of Physics and Astronomy, University of Maryland, College Park, Maryland 20742
(Received 9 February 1976)

Two hydrogen n-α transitions, $n = 13 \rightarrow 12$ at $\lambda 88.7$ μm and $n = 12 \rightarrow 11$ at $\lambda 69.0$ μm, were observed in a large-diameter θ discharge at electron densities between 10^{14} and 3×10^{14} cm^{-3}. Line profiles were measured with a Czerny-Turner infrared monochromator and a Ge:Ga photodetector at liquid-helium temperature. Both n-α lines exhibit strong and symmetric satellite features, with intensities comparable to their parent lines and displacements close to the electron plasma frequency ω_p. These satellites can be interpreted in terms of plasmon-atom collisions if long-wavelength fluctuations in this turbulent plasma are enhanced by a factor $\gtrsim 10^3$ above the thermal level at $T_e \simeq 0.7$ eV. As an independent estimate for the level of turbulence, the continuum emission in the regions corresponding to ω_p and $2\omega_p$ was measured, and found to be well above the level expected for a thermal plasma. Comparison with fluid theory, after radiative transfer corrections, shows satisfactory consistency with the n-α satellite diagnostics.

I. INTRODUCTION

Stark broadening of spectral lines has long been considered as a very reliable and powerful plasma diagnostic method, mainly because of its wide range of applicability and the relatively simple, nonperturbing experimental procedure. A large amount of work[1] has been devoted to the case of a *thermal* plasma, where the dominant particle-produced fields (electrons and ions) are well interpreted, based on two practical and complementary approximations, quasistatic[2] and impact.[3,4] For the case of *turbulent* plasma, in which wave-like fields are no longer negligible, especially when long-wavelength fluctuations are highly enhanced over their thermal level, the *turbulent* Stark profile must be separately investigated[1,5] and then convolved with the *thermal* Stark profile, should they be statistically independent.

If the Stark shifts resulting from the enhanced wave field are larger than any of the characteristic frequencies of the plasma, or at least larger than those for which the enhancement is significant, the quasistatic approximation may well be adequate. The problem is then reduced to predicting distribution functions for the instantaneous value of this wave-produced electric field.[6] A number of general theoretical considerations[7,8] have fallen into these categories, accompanied by many experiments dealing with hydrogen Balmer lines[9-15] or ionized helium lines[16] to demonstrate this additional Stark broadening.

For the cases where Stark shifts are comparable to the relevant plasma frequencies, much less work has been done. There have been some reports of weak plasma satellites, corresponding to the electron plasma frequency or its multiples, on Balmer lines in turbulent heating experiments.[17,18] This paper, however, presents a different theoretical approach and provides the first experimental evidence for a pair of satellites, equally strong as their parent line, on the Stark profiles of hydrogen n-α lines in turbulent plasma.[19] Baranger and Mozer's description of plasma satellites as two quantum (plasmon + photon) transitions[20] in forbidden lines seems unsuccessful here because of the degeneracy of hydrogen, and one would anticipate a more complicated structure. Time-varying Stark effects on a degenerate system had been studied as early as 1933 by Blochinzew,[21] and recently reapproached by Bakshi *et al.*[22] and Hicks,[23] considering a harmonic field superimposed on a static field. Multisatellites at different harmonics were predicted, and none of the above theories shows much analogy to the present experiment.

As an initial step to solve this dilemma, we consider, instead of assigning a single frequency and a constant amplitude, a superposition of normal modes of the field having a spectrum of certain frequency spread and amplitude variation. For a strongly turbulent plasma, waves are excited and annihilated through nonlinear mechanisms. Despite the long-range Landau damping, a stationary plasma state[24,25] could be formed, and there could be plasmon collisions with the radiating hydrogen atoms. The frequency spread and the enhancement factor of the plasma waves determine position and magnitude of the optical satellites.

Two n-α transitions, $n = 13 \rightarrow 12$ at $\lambda 88.7$ μm and $n = 12 \rightarrow 11$ at $\lambda 69.0$ μm, were measured via grating spectroscopy. A photoconductive Ge:Ga detector with a first-stage preamplifier was embedded in liquid helium to optimize the sensitivity as well as the time response. In contrast to our earlier measurement,[26] satellites were observed on both

n-α lines under a turbulent plasma condition at $N_e = (1-3) \times 10^{14}$ cm^{-3} and $T_e \simeq 0.7$ eV.

As an independent diagnostic test, continuum radiation at frequencies corresponding to the plasma frequency ω_p and its harmonic $2\omega_p$ was also measured. Mesh filter combinations and an InSb detector were used, and the bremsstrahlung was found to be well above the level expected for a thermal plasma. Radiative transfer was included in the comparison with the two-fluid magnetohydrodynamic theory.[27] The results show significant enhancement of fluctuating electric field energy by a factor $\gtrsim 10^3$ above the thermal level. This is in agreement with the n-α-line spectroscopy, which suggests that the bandwidth of the enhanced fluctuations is about 10% of the plasma frequency.

Section II will describe the experimental method, especially emphasizing the infrared-detector operation; Sec. III will give the theoretical background; finally, a detailed analysis of the turbulent Stark profiles and the enhanced field fluctuations will be presented in Sec. IV.

II. EXPERIMENTAL METHOD

A. General description

The main body of the light source is a cylindrical glass tube with 46 cm i.d. and 330 cm length, evacuated to 6×10^{-6} Torr and encircled by a 50-cm-i.d. 1-m-long single-turn coil. The plasma was generated by discharging two capacitor banks through the main coil. A "bias" bank (56 μF, 11.2 kJ), charged up to 8 kV, was fired initially, and at its first current peak, was shorted by an evacuated "crowbar" switch. This provided a slowly decaying bias magnetic field in the range of 200 to 100 G. A 1-μF 100-kV low-inductance capacitor bank was discharged simultaneously with the bias crowbar switch, and created a rapidly time-varying magnetic field with a ringing frequency of 140 kHz and a damping constant of 20 μsec (see Fig. 1). With purified hydrogen gas (> 99.999%) maintained at 15 mTorr, a plasma was obtained at electron density $N_e = (1-3) \times 10^{14}$ cm^{-3} and electron temperature $T_e \approx 0.7$ eV for times ≥ 30 μsec from the 100-kV discharge.

The plasma was diagnosed mainly by a 0.5-m Jarrell-Ash monochromator which views end on and can be moved vertically. This gives a measurement of the average electron density along the line of sight from H_δ Stark profiles. By changing to wider slit combinations, it also provides an estimate of electron temperature from the total line intensity ratios of H_β, H_γ, and H_δ. Figure 1 shows the temporal development of the space-averaged electron density and electron temperature, with experimental errors of 10–20%.

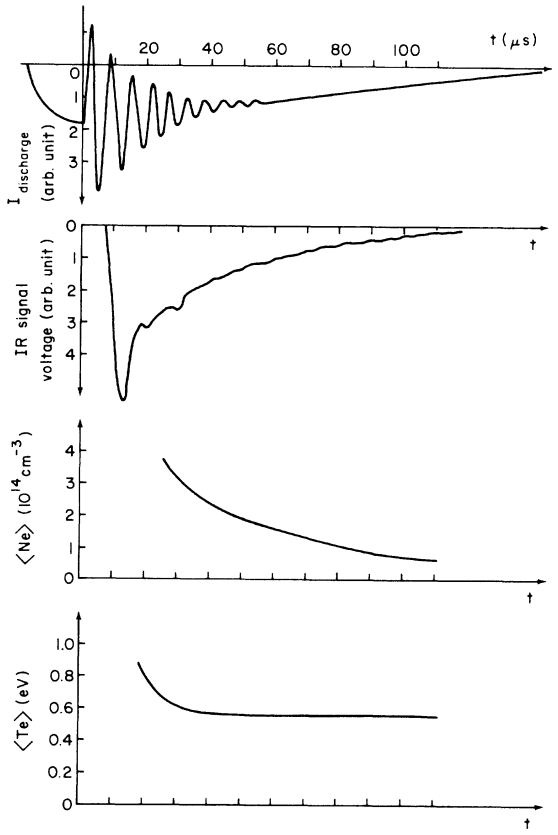

FIG. 1. Temporal development of discharge current, infrared signal, space-averaged electron density, and space-averaged electron temperature.

B. Far-infrared detecting system

1. Monochromator and guiding system

The details of the infrared monochromator and the guiding system have not changed much compared to the previous experiment.[26] A special echelette main grating, with 100 μm groove spacing and 90° edging (from Advanced Kinetics, Inc.) provided an optimum first-order dispersion in the 50–120 μm region. The actual f number of the monochromator (also from Advanced Kinetics, Inc.) is designed to be approximately $f/3$, corresponding to an accepted angular divergence of ~23°.

The far-infrared radiation was collected by a 2-ft-long brass cone with 3.70-in. entrance diameter and 0.935-in. exit diameter, located on the central axis and 32 cm away from the coil edge. This provided an average acceptance region up to 10 cm in radius, covering most of the central part of the cylindrical plasma column. A polyethylene window was used as the vacuum seal for the whole guiding system, which consists of brass circular pipes and brass 90° bends, as well as

brass condensing cones. Because of the very low photon energy of far-infrared radiation, high resolution must be sacrificed to obtain an adequate transmission of energy, especially in the case of our transient plasma, where lock-in techniques cannot be applied. The infrared monochromator as well as the guiding system were evacuated to avoid any water-vapor absorption, and instead of using an inefficient grating filter and mesh filter combination, we simply put in plane mirrors. The necessary second-order-harmonics filtering was accomplished by liquid-helium-cooled "supertransmission" crystals which will be described later.

In order to put the infrared detector into the commercial-size liquid-helium Dewar, the light pipe had to be tapered from the nominal 1 in. diameter down to 0.385 in., and in order to obtain the optimum illumination onto the photoconductive crystal a second light-condensing system is required. These two condensing cones were carefully designed such that their f numbers and the f number of the monochromator are matched to one another. The optimum choices of cone parameters are 6.30 in. long, 0.935-in. entrance diameter, 0.385-in. exit diameter for the first cone, and 1.5 in. long, 0.390-in. entrance diameter, 0.260-in. exit diameter for the second cone, based on Williamson's criterion.[28]

Supertransmission properties, i.e., steepening of the transmittance characteristic curve when cooled to liquid-helium temperature, exist on many crystals,[29,30] especially the halide compounds. In this experiment we use z-cut crystal quartz as filtering material in the region 40–80 μm, and sodium chloride in the region 65–120 μm.

2. *Photoconductor and bias circuitry*

The use of germanium crystals doped with shallow impurities for far-infrared detectors has been known for many years.[31-34] For our experiment, a typical gallium-doped germanium crystal, with impurity ionization energy of 0.0108 eV corresponding to a long-wavelength cutoff of 115 μm, was obtained from Moore and Shenker.[35] With dopant concentration around 9×10^{13} cm^{-3}, Hall mobility of 2×10^{5} cm^2 V^{-1} sec^{-1} at 4.2 °K, and recombination times on the order of 10^{-8} sec. this detector provides a fairly good normalized detectivity $D^*=3.1\times10^{11}$ cm Hz$^{1/2}$ W^{-1} [or a noise equivalent power (NEP) of 8×10^{-13} W Hz$^{-1/2}$]. Physically, the sample is 8.3 mm long and 1.3×1.4 mm^2 in cross section. The bias voltage is applied across the long dimension of the detector.

The bias circuitry is shown in Fig. 2. The lead-out wire is doubly insulated (enameled and cotton wound) No. 40 Advance, which has low thermal

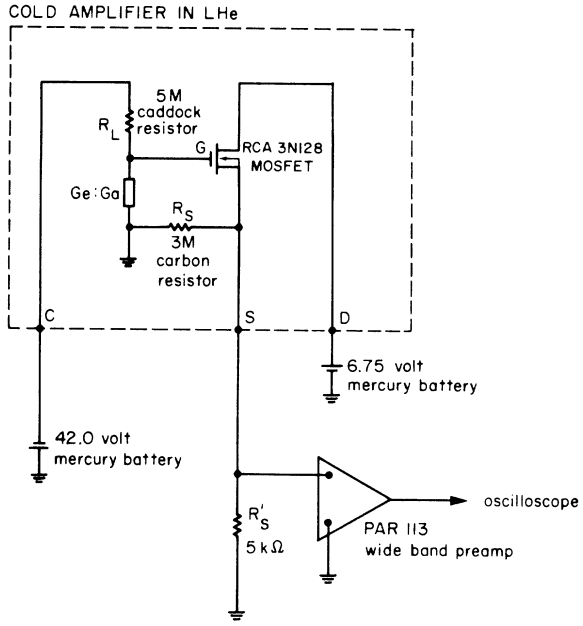

FIG. 2. Ge:Ga photocrystal and cold amplifier bias circuitry.

and low electrical conductivities ($\simeq 50$ Ω/ft). The load resistor is a 5-MΩ metal-oxide-film resistor manufactured by Caddock Industries. Its resistance increases by 80% to 9 MΩ when cooled to 4.2 °K. Both ends of the Ge:Ga crystal were freshly etched with a 1 HF:4HNO_3 solution,[36] and then carefully covered by an indium alloy solder (90% indium, 10% gallium[37]). This procedure is so delicate that a fine-temperature-controlled solder gun is required, and as a major factor in the detector noise, the contact between crystal and this boundary layer of solder has to be good. With pure indium solder, the sample was then mounted in an integrating cavity at the bottom of the helium Dewar.

A Duracell mercury battery provides a very stable bias current ($\simeq 4$ μA); and with the effective dc detector resistance $R_D \simeq 0.5$ MΩ, the voltage δV across the crystal is given by Putley[32] as

$$\delta V = \frac{R_L R_A h\,\xi}{(R_L+R_D)(R_A+R_L)R_D}\,\delta\phi\,, \tag{2.1}$$

where $\delta\phi$ is the photon flux, $R_A=(\partial V/\partial I)_\phi$, R_L is the load resistance, R_D the detector resistance, ξ the bias supply voltage, and $h=-(\partial R_D/\partial\phi)$, measured at constant bias voltage. This output voltage is first connected to a liquid-helium-cooled preamplifier, and then leads out of the Dewar to a low-noise PAR-113 preamplifier with 100 MΩ input impedance, 15 pF input capacitance, and 600 Ω output impedance.

3. Liquid-helium-cooled preamplifier

With crystal impedance in the order of $10^5\ \Omega$, a stray capacitance of only 50 pF could reduce the net signal plus noise by a factor of 10 for the 100-kHz Fourier component. This limits the time response of our detector to 20 μsec. To improve this situation, we used a MOSFET (metal-oxide-semiconductor field-effect transistor) in a source-follower configuration (see Fig. 2), also placed in liquid helium. This decreases the output impedance from $10^5\ \Omega$ to several kΩ, allowing leads of a few feet in length to couple the signal out of the Dewar.

An RCA 3N128 MOSFET was chosen because of its small size and very low power dissipation.[38-40] Bias supply (+6.75-V Burgess mercury battery) and source resistor (5 kΩ, carbon) are contained in a metal box kept at room temperature. Inasmuch as any high transient voltage or any heat-bath contact could cause permanent damage to the device, a number of special precautions were essential.[41]

4. Resolution and wavelength calibration

It was found that under appropriate conditions a lasing transition of neutral helium ($3\,^1P_1 \rightarrow 3\,^1D_2$) at 95.8 μm could be observed in this device.[42] By scanning over this line, on a shot-to-shot basis, a rather reliable instrumental profile and single-wavelength calibration could be obtained. To calibrate other wavelengths, absorption lines of hydrogen chloride, at 40.5, 53.7, 60.3, 68.8, 96.0, and 119.9 μm,[43] were scanned. A pressurized mercury (Osram) lamp, with outer glass envelope detached, provided a good source in this region. A short gas cell containing a small amount of HCl was placed in the light path, and with the help of the chopping and lock-in technique the very narrow absorption lines could be measured. The filling pressure of HCl was kept low enough so that the collisional broadening did not dominate the instrumental broadening. We assumed that all broadening except that caused by collisional and instrumental effects is negligible and all HCl absorption lines have approximately the same collisional widths, which could be obtained by deconvolving the 95.8-μm helium laser line profile from the 96.0-μm HCl line profile. The apparatus width for other HCl lines could then be obtained by deconvolving this collisional width from the measured profiles.

The monochromator has an overall focal ratio of about $f/3$ and, with 1-in.-diam light pipes serving as entrance and exit apertures, the resolution was about $\Delta\lambda_{1/2} \simeq 8$ μm. In order to resolve the high n-α lines, a pair of slits $\frac{3}{16}$ in. wide was designed and inserted in vertical slots mounted at the entrance and exit of the main grating compartment. This gives apparatus widths of about 1.15 μm at 69.0 μm and 1.35 μm at 88.7 μm.

5. Time response

The helium laser at 95.8 μm also served for checking the time response of the detector. With no reflecting mirror in the optical system, the maximum duration of this laser pulse should correspond to the transit time of a wave train between the plasma boundaries. The plasma column is 2 m long, implying that the duration of the pulse is on the order of 10^{-8} sec.

With the cooled source follower as first-stage preamplifier, the detector shows a time response as good as 0.36 μsec. After being connected with the wide-band (0.03–300 kHz) PAR-113 preamplifier, the integrating time increases to 0.90 μsec.

6. Sensitivity calibration

The Osram mercury arc is the most efficient and most commonly used continuous radiation source in the far-infrared and submillimeter wavelength region. The fused quartz envelope, highly transparent in the visible region, becomes opaque to radiation of wavelength longer than 5 μm and starts to transmit again between 50 and 130 μm (depending upon thickness), finally reaching high transparency in the submillimeter region. At wavelengths where the quartz is highly transparent, the mercury lamp radiates approximately as a 3000 °K blackbody[44] (the temperature of the mercury plasma); where the quartz is opaque, it radiates as blackbody at the envelope temperature. In the transition region, the characteristic emission will be the superposition of both, $B_{\text{quartz}}(\lambda) + T(\lambda)B_{\text{Hg}}(\lambda)$, where $T(\lambda)$ is the transmission coefficient of the quartz envelope.

To determine where the quartz envelope ceases to be opaque, a relatively hot hydrogen plasma was generated by firing the main discharge and the bias bank simultaneously and letting the latter "ring," instead of being crowbarred. Owing to the small line-to-continuum ratio (proportional to $T_e^{-1}\Delta\lambda_{1/2}^{-1}$), essentially all of the radiation in this wavelength range is bremsstrahlung. For $\hbar\omega \ll \kappa T$, blackbody (Hg lamp) radiation has a $\lambda^{-4}\Delta\lambda_{1/2}$ dependence, while bremsstrahlung goes as $\lambda^{-2}\Delta\lambda_{1/2}$. Therefore by plotting $V_{\text{brem}}/\lambda^2 V_{\text{Hg}}$ against λ, we can easily identify the transition region where the envelope blackbody approximation breaks down.[42] It turns out that up to 100 μm the mercury lamp acts as a blackbody at the fused-quartz-envelope temperature.

Reliable absolute calibration was unobtainable, because the envelope temperature remained un-

certain. However, the ratio $V_p(t)/\lambda^2 V_{Hg}$, with $V_p(t)$ being the infrared signal voltage at time t, will be proportional to the actual line-plus-continuum (dominated by bremsstrahlung) intensity.

7. *Noise figure*

Noise varieties which are unavoidable are generation-recombination (GR) noise, Nyquist noise, $1/f$ noise, and amplifier noise. Careful investigation shows that the detector is limited mainly by background (GR) noise and the MOSFET intrinsic noise, which are together in the range 100–300 μV.

C. Turbulent plasma experiment

1. *Description*

A pure-hydrogen θ discharge plasma was generated following the discharge sequence described in Sec. II A, with discharging voltage of 100 kV and bias magnetic field in the range of 100 to 200 G. The filling pressure was set at 15 mTorr H_2 and carefully maintained within 1% accuracy.

A typical infrared signal is shown in Fig. 1. At the instant of implosion, the plasma could be as hot as 5 to 10 eV and as dense as 10^{15} cm^{-3}, emitting a bremsstrahlung-dominated continuum. The n-α-line profiles started to emerge after 25 μsec, and a series of ir data was taken between 30 and 70 μsec. Data at later times had to be discarded, because of the very poor signal-to-noise ratio. At each wavelength setting, we usually took numerous shots (at least 15 shots in three different runs) and represented the statistical error in the form of "standard deviation of the mean," i.e., $[\sum_i (x_i - \bar{x})^2/N(N+1)]^{1/2}$, with N denoting the number of shots. Either the $\frac{1}{2}$-m or a $\frac{1}{4}$-m visible monochromator was used as the monitor of any significant trends during the long period of a scan (usually 10-12 h).

2. *Measurements of 12-α (88.7 μm) and 11-α (69.0 μm) lines*

The supertransmitting sodium chloride crystal, which blocks all the radiation below 60 μm, was used in scanning the 12-α line. Data obtained at 30 and 50 μsec are plotted in Figs. 3 and 4. With an apparatus resolution of ~1.4 μm, the line profiles clearly exhibit a symmetric satellite structure and the displacement between each satellite and the unshifted line decreases as the plasma decays. [The ~0.8- and ~0.4-μm shifts of the central peaks are probably not significant but rather indicative of the achievable wavelength accuracy with a monochromator designed for a bandwidth of ~8 μm (see also Sec. II B 4).] After converting to the wave-number scale, we find that this splitting is close to the electron plasma frequency. Near 95

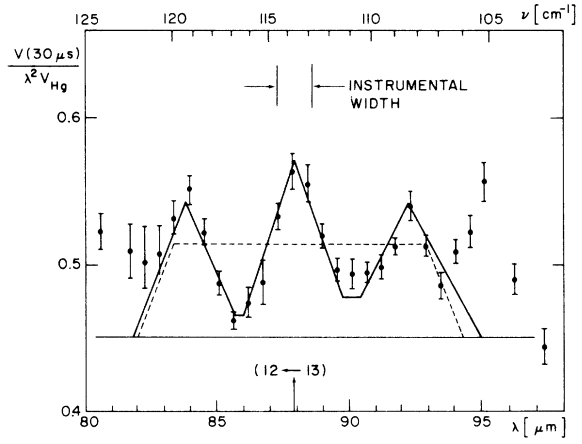

FIG. 3. Hydrogen 12-α-line profile 30 μsec after high-voltage discharge. V and V_{Hg} are signal voltages due to plasma and mercury lamp (blackbody) radiations, respectively.

μm is another peak which does not shift with time (density), probably due to an unidentified impurity line. (The rising trend toward 80 μm may also be caused by an impurity rather than by a satellite whose opposite partner would be near 95 μm, an interpretation supported by the appearance of a peak near 95 μm both in the control experiment discussed in the Sec. II D and our earlier work.[26])

For the 11-α line, we changed the infrared filter to z-cut crystal quartz, whose cutoff wavelength is around 40 μm, and used essentially the same technique as for the 12-α line. The overall sensitivity is a little less in this case. Figures 5 and 6 show

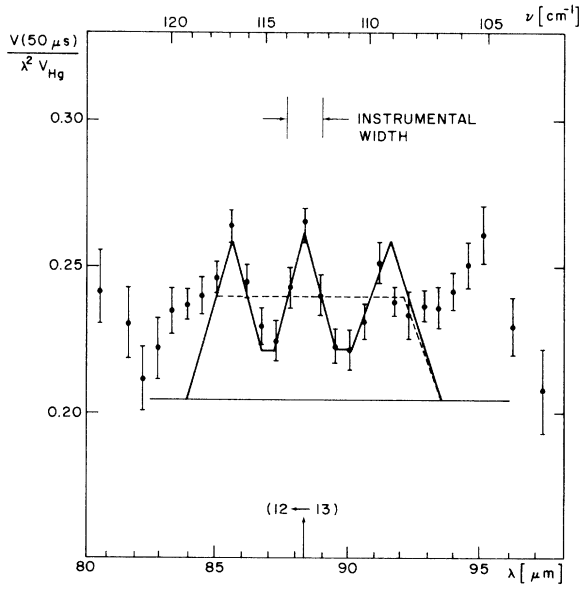

FIG. 4. Hydrogen 12-α-line profile 50 μsec after high-voltage discharge.

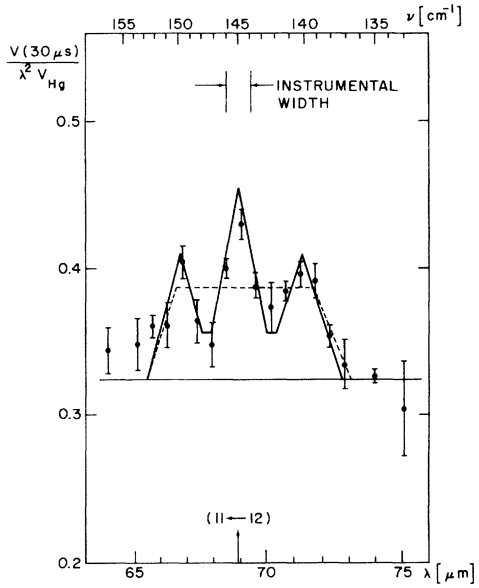

FIG. 5. Hydrogen 11-α-line profile 30 μsec after high-voltage discharge.

the calibrated profiles at 30 and 50 μsec, which again exhibit satellite structure with decreasing displacement but no impurity lines. (In this case the central peaks coincide with the unperturbed line centers to within ~0.1 μm.) Any higher-order satellites are below the experimental threshold for detection (~20% of the unshifted line intensity; see also Sec. IV B 4).

To check the reproducibility, these measurements were repeated half a year later. All features were seen to be reproduced[41] and no significant ($\gtrsim$ 20% of the main line) peaks were found within -6 to $+10$ μm of the 11-α line.

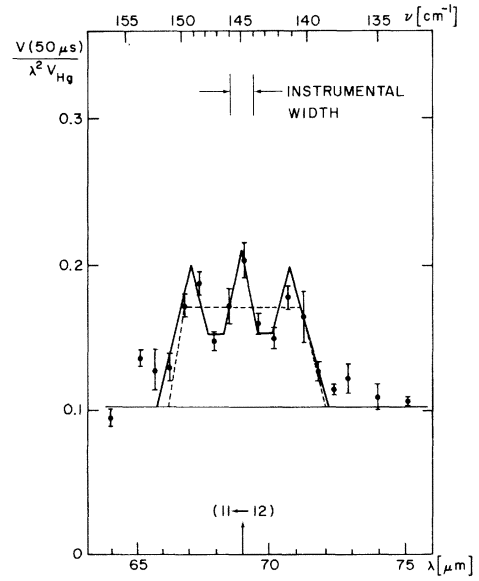

FIG. 6. Hydrogen 11-α-line profile 50 μsec after high-voltage discharge.

D. Control plasma experiment

It was suspected that these satellites are indeed due to a plasma turbulence phenomenon. A control plasma experiment was thus undertaken to investigate the correlation between the plasma field fluctuations and the satellites. A simple way to produce a less turbulent plasma is to increase the damping rate, at least the collisional damping, by using higher fill pressure or by introducing additional impurities. Another approach is the reduction of the external driving field by a decrease in the main discharge voltage.

The pressure was raised first, up to double its usual value, but no significant change occurred before the infrared signal became too weak to be observable. The second approach, however, was successful. After decreasing the discharge voltage by 20% (from 100 to 80 kV), without a large drop in electron density ($N_e = 1-2 \times 10^{14}$ cm^{-3}) and electron temperature ($T_e \approx 0.6$ eV), we observed fairly clear 12-α-line profiles. (The relative smallness of the infrared signal prevented us from measuring the 11-α line.) Six to ten shots were taken at each wavelength position, and the profile in Fig. 7 shows no satellites, consistent with our earlier measurements,[26,42] which also correspond to voltages below 100 kV.

III. THEORETICAL MODEL

For a first attempt at an explanation of the observed line structure, a study of the hydrogen spectrum under the influence of harmonically (in time) varying electric fields,[21] or of such fields combined with quasistatic fields, may seem indicated. The latter case has recently been in-

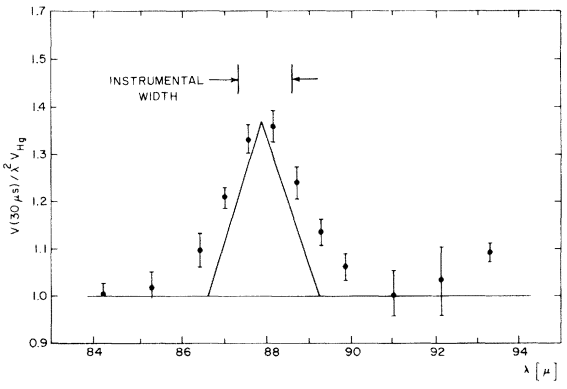

FIG. 7. Hydrogen 12-α-line profile from control plasma (reduced discharge voltage) experiment.

vestigated by Bakshi *et al.*,[22] inclusive of the Zeeman effect from a static magnetic field, but does not seem to correspond to our experimental situation; their theory would give additional satellites at multiples of the electron plasma frequency ω_p from line center for satellites near ω_p as strong as those we observe. Similarly, attempts to extend Baranger and Mozer's description[20] of plasma satellites as two-quantum (photon and plasmon) transitions from helium lines to (degenerate) hydrogen lines are not likely to succeed either, because they should result in more complicated structure as well.

We believe that the answer to this dilemma of having strong plasma satellites without significant higher harmonics is connected with the fact that electric fields in turbulent plasmas are not very well represented by a single-frequency, constant-amplitude, field. Rather, we have a superposition of single-mode fields, say at $\vec{x}=0$,

$$\vec{E}(t)=\mathrm{Re}\sum_{\vec{k}}\vec{E}_{\vec{k}}e^{-i(\omega_{\vec{k}}+i\gamma_{\vec{k}})t}. \tag{3.1}$$

Here $\vec{E}_{\vec{k}}$ stands for the $\vec{k}$th spatial Fourier component of the field at time $t=0$, and $\omega_{\vec{k}}$ and $\gamma_{\vec{k}}$ are real and imaginary parts of the complex frequency of the appropriate eigenmodes of the plasma (which will be assumed to be isotropic). In other words, the field has a frequency spectrum and the various modes grow or decay in time, the growth of course being limited by some nonlinearity.[24,25]

These general properties of the perturbing field invite the use of the impact approximation to the unified line-broadening theory[45] of Smith *et al.* and Voslamber, namely, according to Eqs. (282) and (358) of Ref. 1,

$$L(\omega)=-\pi^{-1}\,\mathrm{Im}\,\mathrm{Tr}\Delta_d[\omega-\mathfrak{L}(\omega)]^{-1} \tag{3.2}$$

(in angular frequency units), with

$$\mathfrak{L}(\omega)\approx -i\frac{e^2}{3\hbar^2}\left(\sum_{i''}\vec{r}\,|i''\rangle\cdot\langle i''\,|\vec{r}-2\vec{r}_i\cdot\vec{r}_f^{\,*}+\sum_{f''}\vec{r}_f^{\,*}\,|f''\rangle\cdot\langle f''\,|\vec{r}_f^{\,*}\right)\int_0^\infty e^{i\omega t}[\vec{E}(t)\cdot\vec{E}(0)]_{\mathrm{av}}\,dt\,, \tag{3.3}$$

if we restrict our attention to completely degenerate atomic levels, count frequencies from the unperturbed line position, and make the dipole approximation ($\vec{k}\cdot\langle i|\vec{r}|i'\rangle\ll 1$). Δ_d generates the appropriate relative strengths of the various components of the line. In Eq. (3.3) $\vec{r}$ is the position vector operator of the atomic electron, and the sums over i'' and f'' are over all substates of the upper and the lower levels of the line. The average in the field autocorrelation function is over all plasma modes designated by their wave vectors $\vec{k}$. Essentially, the coming (growth, $\gamma>0$) and going (decay, $\gamma<0$) of the eigenmodes in a turbulent plasma is treated analogously to the transient nature of particle-produced fields (especially by electrons) for which the impact approximation was originally developed.[3,4] The validity of this crucial approximation needs special scrutiny for the present situation (see Sec. IV A 5).

From Eq. (3.1) and the random-phase assumption, follows for the autocorrelation function of the wave-produced electric field,

$$[\vec{E}(t)\cdot\vec{E}(0)]_{\mathrm{av}}=\frac{1}{4}\left(\sum_{\vec{k}}\vec{E}_k\cdot\vec{E}_k^{\,*}e^{-i(\omega_k+i\gamma_k)t}+\mathrm{c.c.}\right) \tag{3.4}$$

and therefore for its Laplace transform

$$\lim_{T\to\infty}\int_0^T e^{i\omega t}[\vec{E}(t)\cdot\vec{E}(0)]_{\mathrm{av}}\,dt = \frac{i}{4}\sum_{\vec{k}}\vec{E}_k\cdot\vec{E}_k^{\,*}\lim_{T\to\infty}\left(\frac{1-e^{i(\omega-\omega_k-i\gamma_k)T}}{\omega-\omega_k-i\gamma_k}+\frac{1-e^{i(\omega+\omega_k-i\gamma_k)T}}{\omega+\omega_k-i\gamma_k}\right). \tag{3.5}$$

Because of the profile symmetry, we omit the terms involving $\omega+\omega_k$; because of the dense spectrum of Langmuir modes, we replace $\sum_{\vec{k}}$ by $V\int d^3k/(2\pi)^3$. Also assuming $|\gamma_k|\ll\omega_k$ and isotropy, Eq. (3.5) can be rewritten by using

$$\int f(k)\lim_{T\to\infty}\frac{1-e^{i(\omega-\omega_k-i\gamma_k)T}}{\omega-\omega_k-i\gamma_k}\,dk=\int_{\omega_1}^{\omega_2}g(\omega_k)\lim_{T\to\infty}\frac{1-e^{i(\omega-\omega_k-i\gamma_k)T}}{\omega-\omega_k-i\gamma_k}\,d\omega_k \approx i\pi\frac{\gamma}{|\gamma|}\,g(\omega)+\mathrm{P}\int_{\omega_1}^{\omega_2}\frac{g(\omega_k)}{\omega-\omega_k}\,d\omega_k-g(\omega)\int_{x_1}^{x_2}\frac{(x+i\eta)e^{ix+\eta}\,dx}{x^2+\eta^2}\,, \tag{3.6}$$

with $(\omega-\omega_k)T=x$ and $\gamma_k T=\eta$ in the last (error) term.

For an estimate of the error term, we simply assume that $g(\omega_k)$ vanishes sufficiently rapidly at the boundaries (ω_1,ω_2) of the plasma spectrum and is slowly varying elsewhere, so that it can be taken outside of the integrand. From Eqs. (5.1.41), (5.1.42), and (5.1.51) in the *Handbook of Mathemat-*

ical Functions,[46] we have

$$\int_{x_1}^{x_2} \frac{(x+i\eta)e^{ix+\eta}\,dx}{x^2+\eta^2} = -\left[E_1(-\eta - ix)\right]_{x_1}^{x_2} \approx e^{\eta}\left(\frac{e^{ix_2}}{ix_2+\eta} - \frac{e^{ix_1}}{ix_1+\eta}\right) = i\,\frac{e^{\gamma T}}{T}\left(\frac{e^{i(\omega-\omega_1)T}}{\omega-\omega_1-i\gamma} - \frac{e^{i(\omega-\omega_2)T}}{\omega-\omega_2-i\gamma}\right). \tag{3.7}$$

If the width of the plasma spectrum is $\Delta\omega_p$, the above error term is typically of order $e^{\gamma T}/\Delta\omega_p T$ or less. For decaying modes ($\gamma<0$) this vanishes in the limit $T\to\infty$, but for growing modes it would seem to diverge. However, $e^{2\gamma T}$ must be limited by the enhancement factor A of the electrical energy density over the thermal level, and $|\gamma| \ll \Delta\omega_p \leq \omega_k$ should hold for most frequencies of interest.

It is therefore rather safe to conjecture that except for the sign of the real part, decaying and growing modes give identical contributions to the Laplace transform of the electrical field autocorrelation function, provided for growing waves the condition

$$2A^{1/2}\gamma/\Delta\omega_p\,(\ln A) \ll 1 \tag{3.8}$$

is fulfilled. For stationary turbulence, should such a plasma state exist,[24,25] the energy densities associated with growing and decaying modes are about equal at all relevant frequencies, and the real parts will cancel. Eq. (3.5) then reduces to

$$\int_0^{\infty} e^{i\omega t}\left[\vec{E}(t)\cdot\vec{E}(0)\right]_{av} dt \simeq \frac{i}{4}\,\mathrm{P}\int \frac{|\vec{E}_k|^2}{\omega-\omega_k}\,\frac{V}{(2\pi)^3}\,4\pi k^2\,\frac{dk}{d\omega_k}\,d\omega_k, \tag{3.9}$$

and from Eq. (3.3) we have for the real part of the line-shape operator

$$\mathrm{Re}\mathfrak{L}(\omega) \simeq \frac{e^2 V}{24\pi^2\hbar^2}\,\mathfrak{C}\,\mathrm{P}\int \frac{|\vec{E}_k|^2}{\omega-\omega_k}\,k^2\,\frac{dk}{d\omega_k}\,d\omega_k, \tag{3.10}$$

where $\mathfrak{C} = (\sum_{i''}\cdots)$ as in Eq. (3.3), anticipating that the wave contribution ($k<1/\rho_D$) to $\mathrm{Re}\mathfrak{L}(\omega)$ will be much larger than the particle contribution ($k>1/\rho_D$) for the condition of our experiment.

Before going on, we note that the absence of a real part in the Laplace transform of the autocorrelation function does not mean that the spectral density of the field has to vanish as well. The Wiener-Khintchine theorem would seem to impose such severe restriction, i.e., to point out an inconsistency in our theoretical model. However, for fields as described by Eq. (3.1), the function $C(t) = [\vec{E}(t)\cdot\vec{E}(0)]_{av}$ does not necessarily fulfill the conditions[47] for the Fourier inversion theorem underlying the above theorem. [Note that $C(t)$, as it stands, is not square integrable on the interval $t=0,\infty$ unless all γ's fulfill $\gamma_k<0$.] To complete our model, we should limit the growth of modes also in the present context by some cutoff *and* provide for the generation of new modes. Depending on the details of these processes, there will then be additional contributions to the spectral density, etc., but it seems reasonable to assume that they would be outside the frequency range where the imaginary part of the Laplace transform of $[\vec{E}(t)\cdot\vec{E}(0)]_{av}$ is significant.

The apparent inconsistency mentioned above could therefore most likely be resolved, but we would be amiss not to stress that the existence of stationary Langmuir turbulent plasma states is an open question. Perhaps there would be rather large fluctuations in their spectra, an effect suggested by some of the theoretical models,[48-50] a detailed discussion of which is well beyond the scope of this paper. We again surmise that such fluctuations are of sufficiently low frequency to be neglected, because they are neither resolvable experimentally nor even in principle able to survive the damping effect (on the observed lines) from particle-produced fields (see below).

In a turbulent plasma, the total energy for a single mode may be enhanced by a large factor over the thermal excitation level κT (derived from the classical equipartition theorem), namely,

$$V\vec{E}_k\cdot\vec{E}_k^*/8\pi = \kappa T A(\omega_k), \tag{3.11}$$

where $A(\omega_k)$ specifies the approximate nature of the Langmuir wave spectrum, and the dispersion relation is

$$\omega_k^2 = \omega_p^2\left[1+3(k\rho_D)^2+\cdots\right]. \tag{3.12}$$

We now make a model for $A(\omega_k)$, which should have a strong maximum ($A\gg1$) near, but somewhat above, ω_p, say at ω_0, and be small at the boundaries of the spectrum, i.e., $A(\omega_p)=A(\omega_{max}) \simeq 1$. Equation (3.10) then becomes

$$\mathrm{Re}\mathfrak{L}(\omega) \simeq \frac{4Ne^4}{4\sqrt{3}\,\hbar^2}\left(\frac{m}{\kappa T}\right)^{1/2}\mathfrak{C} \times \mathrm{P}\int_{\omega_p}^{\omega_{max}} \frac{(\omega_k^2-\omega_p^2)^{1/2}\omega_k}{(\omega-\omega_k)\omega_p^2}\,A(\omega_k)\,d\omega_k. \tag{3.13}$$

Let us rearrange the integrand and postulate an analytic form,

$$\frac{(\omega_k^2-\omega_p^2)^{1/2}\omega_k}{\omega_p^2}\,A(\omega_k) = \frac{a}{(2\pi)^{1/2}}\exp\left[-\frac{1}{2}\left(\frac{\omega_k-\omega_0}{\Delta\omega}\right)^2\right]. \tag{3.14}$$

[To assess the model sensitivity of our analysis we have also considered a Lorentzian form (see below.)] Provided $\omega_0 - \omega_p$ is much larger than $\Delta\omega$, but still smaller than ω_p, this leads to

$$\mathrm{Re}\mathfrak{L}(\omega) \simeq \frac{4Ne^4}{9\sqrt{3}\hbar^2}\left(\frac{m}{\kappa T}\right)^{1/2} \mathfrak{C}\,\frac{a}{(2\pi)^{1/2}} \times \mathrm{P}\int_{-\infty}^{\infty} \frac{1}{z-x}\, e^{-x^2/2}\,dx\,, \tag{3.15}$$

with

$$z = (\omega - \omega_0)/\Delta\omega\,, \quad x = (\omega_k - \omega_0)/\Delta\omega\,. \tag{3.16}$$

(The condition $\omega_0 - \omega_p >> \Delta\omega$ can probably be relaxed in view of nonlinear frequency shifts and the schematic nature of the postulated plasma spectrum.) Because $(z-x)^{-1} = z^{-1}[1 - x(x-z)^{-1}]$, the integral in Eq. (3.15) is closely related to the $W(z)$ function,[51]

$$W(z) \equiv \frac{1}{(2\pi)^{1/2}} \int_{-\infty}^{\infty} \frac{x}{x - z - i\xi}\, e^{-x^2/2}\,dx\,. \tag{3.17}$$

Using

$$\mathrm{Re}W(z) = 1 - ze^{-z^2/2}\int_0^z e^{x^2/2}\,dx\,, \tag{3.18}$$

we have

$$\mathrm{Re}\mathfrak{L}(\omega) \simeq \frac{4Ne^4}{9\sqrt{3}\hbar^2}\left(\frac{m}{\kappa T}\right)^{1/2} \mathfrak{C}\, ae^{-z^2/2} \times \int_0^z e^{x^2/2}\,dx\,. \tag{3.19}$$

Assuming the error term in Eq. (3.6) is small in comparison with $\mathrm{Im}\mathfrak{L}(\omega)$ for $k > 1/\rho_D$, it remains only to consider the particle (electron) contribution to $\mathrm{Im}\mathfrak{L}(\omega)$, i.e., according to Eq. (361) of Ref. 1,

$$\mathrm{Im}\mathfrak{L}(\omega) \simeq \tfrac{8}{3}\,(\tfrac{1}{2}\pi)^{1/2}\,(Ne^4/\hbar^2)\,(m/\kappa T)^{1/2} \times \mathfrak{C}[\ln(k_m\rho_D) + \tfrac{1}{2}]\,, \tag{3.20}$$

where k_m corresponds to the inverse of the maximum impact parameter below which second-order perturbation breaks down , and where the term $\frac{1}{2}$ accounts for strong collisions, and to specify the $\vec{r}$ matrix elements in $\mathfrak{C}$. For the lower Balmer lines, these elements are very much dependent on angular quantum number l. The resonance condition discussed below [see Eq. (3.24)] regarding the maximum of $A(\omega_k)$ is therefore at best fulfilled only for one of the relevant matrix elements, and there would be only a relatively weak satellite near, but slightly beyond, ω_p from line center. However, for the high n-α lines, the l dependence of the matrix elements nearly cancels after allowing for both upper- and lower-state perturbations. In analogy to the broadening of radio-frequency n-α lines by ion impacts, all of this can be accomplished by the replacement[1,52]

$$\mathfrak{C} = \Big(\sum_{i''} \vec{r}_i\,|i''\rangle\cdot\langle i''|\,\vec{r}_i - 2\vec{r}_i\cdot\vec{r}_f^{\,*} + \sum_{f''} \vec{r}_f^{\,*}\,|f''\rangle\cdot\langle f''|\,\vec{r}_f^{\,*}\Big) \to \tfrac{9}{2}\,a_0^2\bar{n}^2 = \tfrac{9}{2}\,(\hbar^2\bar{n}/me^2)^2\,, \tag{3.21}$$

with $\bar{n}$ being the mean value of the two principal quantum numbers involved. We note here that in case of electron-impact broadening of n-α lines results obtained by using averaged matrix elements and a Lorentzian profile differ from detailed calculations[53] using individual matrix elements only by about 10%.

Since we neglect quasistatic broadening by ion-produced fields,[26,41] it is convenient to use the (nlm) representation, in which $\mathfrak{L}(\omega)$ is approximately diagonal.[1] The strong-collision cutoff k_m can, finally, be obtained from Eq. (4.64) of Ref. 1,

$$k_m \simeq mv_e/\bar{n}\hbar\,, \tag{3.22}$$

where v_e is the electron thermal speed $(\kappa T/m)^{1/2}$. In a reduced frequency scale, viz., $\tilde{\nu} \equiv \omega/\omega_p$, $\Delta\tilde{\nu} \equiv \Delta\omega/\omega_p$, and $\tilde{\nu}_0 \equiv \omega_0/\omega_p$, the line profile according to Eq. (3.2), i.e.,

$$L(\tilde{\nu}) = \frac{1}{\pi}\,\mathrm{Tr}\Delta_d \frac{\mathrm{Im}\tilde{\mathfrak{L}}(\tilde{\nu})}{[\tilde{\nu} - \mathrm{Re}\tilde{\mathfrak{L}}(\tilde{\nu})]^2 + [\mathrm{Im}\tilde{\mathfrak{L}}(\tilde{\nu})]^2}\,, \tag{3.23}$$

will exhibit a satellite structure as observed if we have

$$\mathrm{Re}\tilde{\mathfrak{L}}(\tilde{\nu}) = \tilde{\nu} \tag{3.24}$$

at or near $\tilde{\nu}_0$. [A calculation to fourth order in $\vec{E}_k$ would yield another, but smaller, maximum in $\mathrm{Re}\tilde{\mathfrak{L}}(\tilde{\nu})$ near $2\tilde{\nu}_0$, so that the condition for a strong second-order satellite would be inconsistent with a strong first-order satellite. We also note that this resonance condition may be considered a generalization of Lifshitz's result[21] for stochastic single-frequency one-dimensional fields. His $\delta \approx 1$ condition gives ~60% and ~15% for the intensities of first- and second-order satellites.] In order to resolve these satellites, it is further required that $\mathrm{Im}\tilde{\mathfrak{L}}(\tilde{\nu})$ be at most of the same order as $\Delta\tilde{\nu}$. In summary, from our model we obtain

$$\mathrm{Re}\tilde{\mathfrak{L}}(\tilde{\nu}) \approx 9.26\times 10^{-13}\left(\frac{N_e(\mathrm{cm}^{-3})}{T_e(\mathrm{eV})}\right)^{1/2} \bar{n}^2 a S(\tilde{z})\,, \tag{3.25}$$

with

$$S(\tilde{z}) = e^{-\tilde{z}^2}\int_0^{\tilde{z}} e^{x^2}\,dx\,, \quad \tilde{z} = (\tilde{\nu} - \tilde{\nu}_0)/\Delta\tilde{\nu}\sqrt{2}\,;$$

and

$$\mathrm{Im}\tilde{\mathcal{L}}(\tilde{\nu}) \approx 8.56\times 10^{-12}\bar{n}^2\left(\frac{N_e(\mathrm{cm}^{-3})}{T_e(\mathrm{eV})}\right)^{1/2} \times\left[\ln\left(3.80\times 10^{10}\,\frac{T_e}{\bar{n}\sqrt{N_e}}\right)+\frac{1}{2}\right]. \quad (3.26)$$

Three parameters (a, $\tilde{\nu}_0$, $\Delta\tilde{\nu}$) have to be specified empirically. Of these, $\tilde{\nu}_0$ provides no more information than a relative satellite shift. This leaves $\Delta\nu$ as the only free parameter for the line profile, because a is essentially determined through the constraint Eq. (3.24). For typical values of N_e and T_e in this experiment, the line profiles are plotted in Fig. 8, with a chosen such that Eq. (3.24) holds for $\tilde{\nu}\simeq\tilde{\nu}_0$.

The basic validity condition[1,45] for our expressions for Re$\mathcal{L}$ is, in the case of growing modes,

$$\frac{e}{\hbar}\left|\langle i|\vec{\mathbf{r}}|i'\rangle\cdot\int_0^T \vec{\mathbf{E}}_k^q(t)\,dt\right| \approx \frac{\bar{n}a_0 e}{\hbar\omega_p}\,|\vec{\mathbf{E}}_k^q|\,e^{\gamma_k T}\ll 1\,, \quad (3.27)$$

with the understanding that $|\vec{\mathbf{E}}_k^q|$ is the field associated with a sufficiently large number of quasiparticles to reconstruct the mode in question, i.e., covering a frequency range of order γ_k. All other quasiparticles would be uncorrelated, and our criterion would then mean that perturbations caused by the combined effect of correlated quasiparticles are relatively small, as must be required in analogy to the work of Capes and Voslamber.[54]

For $|\vec{\mathbf{E}}_k^q|$ we estimate

$$|\vec{\mathbf{E}}_k^q| \approx \left(\frac{4\pi\hbar\omega_p}{V}\right)^{1/2}\frac{4\pi Vk^2}{(2\pi)^3}\,\frac{dk}{d\omega_k}\,\gamma_k\,, \quad (3.28)$$

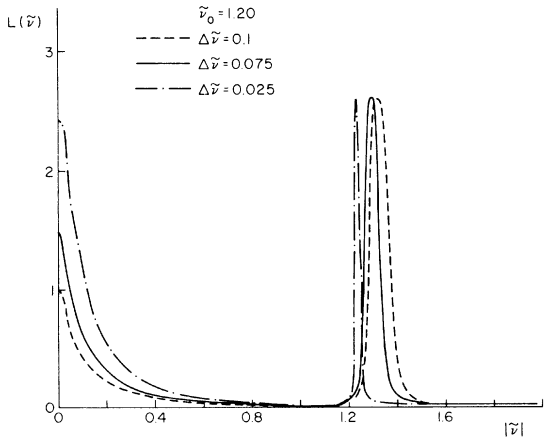

FIG. 8. Calculated turbulent Stark profiles at $N_e\approx 3\times 10^{14}\,\mathrm{cm}^{-3}$, $T_e\approx 0.7$ eV for various width parameters and using the threshold condition.

since the energy associated with a single plasmon is $\hbar\omega_p$ and about half of it is invested in field energy. However, to maintain the semblance of a continuous spectrum, the volume V must obey

$$V^{1/3} > (\Delta k)^{-1} \simeq \left(\gamma_k\,\frac{dk}{d\omega_k}\right)^{-1}. \quad (3.29)$$

The criterion for the validity of the impact approximation thus becomes, again putting $e^{\gamma_k T}\simeq A^{1/2}$,

$$\frac{\bar{n}a_0 ek^2}{\pi^{3/2}(\hbar\omega_p)^{1/2}}\left(\frac{A}{\gamma_k}\,\frac{d\omega_k}{dk}\right)^{1/2} \simeq \frac{\bar{n}}{6}\left(\frac{\hbar}{m}\right)^{3/2}\left(\frac{m}{\kappa T}\right)^{3/4} N_e^{1/2}\,\frac{\omega_k^2-\omega_p^2}{\omega_p^2} \times\left(a\,\frac{\omega_p}{\gamma_k}\right)^{1/2}\exp\left[-\frac{1}{4}\left(\frac{\omega_k-\omega_0}{\Delta\omega}\right)^2\right]\ll 1\,. \quad (3.30)$$

IV. EXPERIMENTAL RESULTS

A. Turbulent plasma experiment

1. Data analysis

All of the $n-\alpha$ line data were fitted to a "triplet" profile, $T(\nu_i)$, which is composed of a main triangle accompanied by two identical triangles displaced symmetrically with respect to the central one. Least-squares techniques were employed to determine the five parameters involved in this unnormalized profile, namely, l, the satellite displacement, h', the satellite height, b', the satellite width, h, the central line height, and b, the central linewidth. We then define the square of the standard deviation σ for the measured intensities I_i as

$$\sigma^2 = \frac{1}{N-1}\sum_{i=1}^{N}\left[(I_i - C) - T(\nu_i)\right]^2\,, \quad (4.1)$$

where N is the number of the shots and C is the continuum intensity, assumed independent of wavelength.

By least-squares "linear" curve fitting to the line-wing data, the continuum intensity C was estimated, and the best-fit parameter set (l, b, h, b', h') was then found through a repeated multidimensional iteration process to minimize σ^2. There is some ambiguity in determining the continuum C, although judging from the facts that both b and b' cannot be less than the apparatus width, and that they will decrease as C increases, we can easily set an upper bound for C. A practical lower bound follows from the lowest signals, and it is found that the satellite displacement l, which decreases with the electron density and is the most interesting quantity in this experiment, is insensitive to the choice of the continuum level as long as C remains close to C_0 within 30%, where

C_0 is the continuum estimated from the "linear" least-squares fitting. This range of the continuum level gives line-to-continuum ratios for the n-α lines which are consistent with the electron temperature as determined from relative Balmer-line intensities.

Because of the inhomogeneity of the plasma along the line of sight, one might actually expect a smoothed, say trapezoidal, profile for these n-α lines. The half-plateau of the trapezoid will then correspond to an average of plasma satellite splittings. As one can see from Figs. 3–6, there is some preference for the "triplet" (solid curve) versus the "trapezoid" (dotted curve) profile. By calculating the minimum σ^2, we found the former shows an edge by a factor of 1.4. By comparing the number of measured data fitted by both profiles (i.e., profile going through the experimental error bars), we again see the "triplet" giving a slightly better agreement with the experimental results. In any event, the profile structure is substantially different from predicted shapes for Stark profiles in thermal plasmas,[26,42] and the existence of strong satellite peaks in an equivalent homogeneous plasma is well supported by these data.

2. *Line shifts caused by plasma wave field*

Table I lists the comparison between the electron plasma frequencies and the satellite displacements for four different cases. (Cases 1 and 3 were taken at 30 μsec and cases 2 and 4 at 50 μsec.) Both 11-α and 12-α lines yield consistent results for these two quantities. All of the half-plateaus of the trapezoids also lie in the vicinity of the plasma frequencies, which further convinces us that this splitting (or broadening) is really a plasma effect. The electron densities are from the Stark broadening of the H_δ line, which is so broad that turbulent Stark broadening could be accounted for by the quasistatic approximation. Since thermal Stark broadening by electrons and ions is comparable and wave- and ion-produced fields are about the same (see Sec. IV A 4), there could be a downward correction in the electron density by, say, a factor of 1.5.

3. *Line broadening caused by particle-produced fields*

According to Refs. 1 and 26, the dominant line-broadening mechanism is due to electron (elastic) collisions. Typical predicted half-(half-widths) from this mechanism are, from Eq. (3.26),

$$\Delta w_{1/2} \simeq \mathrm{Im}\mathfrak{L}(\omega) = \begin{cases} 0.123\omega_p & \text{at } 30\ \mu\text{sec}, \\ 0.108\omega_p & \text{at } 50\ \mu\text{sec}. \end{cases}$$

These values are only 20–30% of the apparatus width, consistent with the narrowness of the triplet profiles.

4. *Estimate of turbulent electric field*

From Eq. (3.23), the normalized line shape is

$$L(\tilde{\nu}) = \frac{1}{\pi} \frac{\mathrm{Im}\tilde{\mathfrak{L}}(\tilde{\nu})}{[\tilde{\nu} - \mathrm{Re}\tilde{\mathfrak{L}}(\tilde{\nu})]^2 + [\mathrm{Im}\tilde{\mathfrak{L}}(\tilde{\nu})]^2}, \tag{4.2}$$

where $\mathrm{Re}\tilde{\mathfrak{L}}(\tilde{\nu})$ and $\mathrm{Im}\tilde{\mathfrak{L}}(\tilde{\nu})$ are given by Eqs. (3.25)

TABLE I. Comparison of the frequency displacements of n-α satellites to the plasma frequencies.

		Case 1 30 μsec	Case 2 50 μsec	Case 3 30 μsec	Case 4 50 μsec
H_δ [a]	$\langle N_e \rangle$ (10^{14} cm^{-3})	3.145	1.80	3.0	1.20
	Error (%)	10	11	15	12
	ω_p (cm^{-1})	5.30	4.0	5.20	3.20
12-α line	$\Delta\nu_s$ [b] (cm^{-1})	5.40	3.75	5.0	2.80
	Error (%)	4	4	5	6
	$\frac{\Delta\nu_t}{\Delta\nu_s}$ [c]	1.15	1.2	1.16	1.18
11-α line	$\Delta\nu_s$ [b] (cm^{-1})	4.90	3.90	4.90	3.10
	Error (%)	6	5	3	5
	$\frac{\Delta\nu_t}{\Delta\nu_s}$ [c]	1.12	1.23	1.15	1.30

[a] Electron densities from the Stark profile of H_δ may have to be reduced by a factor of ~1.5 to account for turbulent Stark broadening, and the corresponding values of the plasma frequency by ~20%.

[b] $\Delta\nu_s$: satellite displacement from "triplet" best fit.

[c] $\Delta\nu_t$: frequency spread from "trapezoid" best fit.

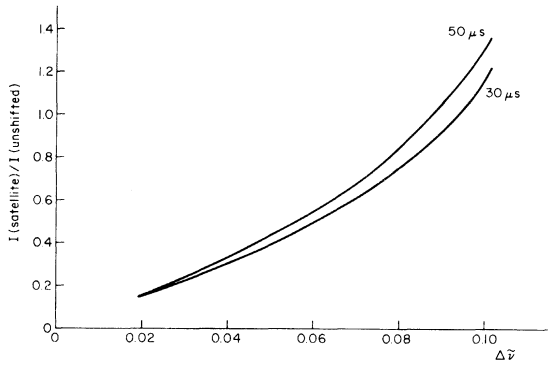

FIG. 9. Calculated intensity ratio between one satellite and the unshifted line as function of the width parameter $\Delta\tilde{\nu}$ of the enhanced plasma spectrum.

and (3.26). As discussed in Sec. III, three parameters, a, $\tilde{\nu}_0$, and $\Delta\tilde{\nu}$, have to be estimated empirically. Since $\tilde{\nu}_0$ specifies only the precise position of the satellite, the line profile is primarily dependent on the choice of $(a, \Delta\tilde{\nu})$. Physically, $\Delta\tilde{\nu}$ denotes the band width of the fluctuating field spectrum, and a represents the average enhancement of its energy density over the thermal level in the band $\Delta\tilde{\nu}$.

Applying the resonance condition (3.24), and choosing $\Delta\tilde{\nu}$ and $\tilde{\nu}_0$ so that $\Delta\tilde{\nu} < \tilde{\nu}_0 - 1$ and $1 < \tilde{\nu}_0 < 1.4$, we calculated the profiles in Fig. 8. The (integrated) intensity ratio between one of the satellites and the unshifted line is given in Fig. 9 as a function of $\Delta\tilde{\nu}$. This ratio can be estimated experimentally from the best fit of "triplet" profiles, and values of $(\Delta\tilde{\nu}, a)$ were thus determined, e.g., for cases 1 and 2 (see Table II). They indicate that the satellites are caused by plasmon-atom collisions, if the long-wavelength plasma field fluctuations are indeed enhanced by a factor of $\sim 10^3$ above the thermal level at $T_e \simeq 0.7$ eV. The actual enhancement could be even larger, overfulfilling the resonance condition, but $\Delta\tilde{\nu}$ would then have to be smaller to fit the data.

The energy density of the fluctuating electric field is given by

$$W_{el} = \frac{1}{2}\int \frac{\vec{E}_k \cdot \vec{E}_k^*}{8\pi} \frac{4\pi k^2\, dk\, V}{(2\pi)^3}\,, \tag{4.3}$$

and from Eqs. (3.11) and (3.14) this can be rewritten

$$W_{el} = \int \frac{\kappa T}{4\pi^2} A(\omega_k) k^2\, dk$$
$$= \frac{N\kappa T}{\pi 3^{3/2}} \frac{e^2}{m}\left(\frac{m}{\kappa T}\right)^{3/2} \frac{a}{(2\pi)^{1/2}}$$
$$\times \int \exp\left[-\frac{1}{2}\left(\frac{\omega_k - \omega_0}{\Delta\omega}\right)^2\right] d\omega_k\,. \tag{4.4}$$

The turbulence level ξ, i.e., the ratio of W_{el} to the average particle thermal energy, is therefore

$$\xi = \frac{W_{el}}{\frac{3}{2}N\kappa T} = \frac{2}{3^{5/2}\pi}\left(\frac{e^2}{\rho_D}\right)\frac{1}{\kappa T}\left(\frac{\Delta\omega}{\omega_p}\right) a\,, \tag{4.5}$$

or, substituting the group of typical parameters for this experiment, $N_e \simeq 3\times 10^{14}$ cm^{-3}, $\rho_D \simeq 0.30$ μm, $\kappa T \simeq 0.7$ eV, $a \simeq 1000$, $\Delta\omega/\omega_p \simeq 0.085$,

$$\xi \simeq 2.6\times 10^{-2}\,. \tag{4.6}$$

From W_{el} we can estimate the root mean square of the fluctuating field,

$$\langle E^2\rangle^{1/2} \equiv (8\pi W_{el})^{1/2} \simeq 5.7\,\text{kV/cm}\,, \tag{4.7}$$

and regard it as a characteristic field strength of the plasma turbulence. This is a fairly reasonable magnitude if we recall the 100-kV discharging voltage and the 10–15-cm radial dimension of the plasma column. The average particle-produced (Holtsmark) field[1,2] is

$$\bar{E}_p \simeq 8.8eN^{2/3} \simeq 5.8\ \text{kV/cm}\,. \tag{4.8}$$

We see that the fields are comparable, which is very unlike the thermal case. If we replace Eq. (3.14) by a Lorentzian, $a'(\Delta\omega')^2/\pi[(\omega_k - \omega_0)^2 + (\Delta\omega')^2]$, we find $a' \approx \sqrt{2}\,a$ and $\Delta\omega' \approx \Delta\omega/\sqrt{2}$, i.e., the same turbulence level and rms field. In Eq. (3.25) the function $S(\tilde{z})$ becomes $\tilde{z}'(\tilde{z}'^2+1)$ with $\tilde{z}' = (\tilde{\nu} - \tilde{\nu}_0')/\Delta\tilde{\nu}'$. [Note that the maximum of this new function is about twice as broad as that of $S(\tilde{z})$.]

5. *Validity of the plasmon impact approximation*

Under the same experimental parameters as in Sec. IV A 4, we have considered the validity criterion for the impact approximation, rewriting Eq. (3.30) as

TABLE II. Values of width parameter $\Delta\nu$ and enhancement factor a.

	$\frac{I_{\text{satellite}}}{I_{\text{unshifted}}}$	ν_0	$\Delta\tilde{\nu}$ (from Fig. 9)	a	N_e (10^{14} cm^{-3})	T_e (eV)
Case 1 (30 μsec)	0.70 ± 0.05	1.20	0.080	940	3.14	0.7
Case 2 (50 μsec)	0.90 ± 0.05	1.20	0.085	1000	1.8	0.5

$$7\times10^{-3}\left(\frac{\omega_p}{\gamma_k}\right)^{1/2}\frac{\omega_k^2-\omega_p^2}{\omega_p^2}\exp\left[-\frac{1}{4}\left(\frac{\omega_k-\omega_0}{\Delta\omega}\right)^2\right]\ll 1. \tag{4.9}$$

For $\omega_k\simeq\omega_0\simeq 1.2\omega_p$ and $\gamma_k\simeq 10^{-3}\omega_p$, which are very reasonable in the present case, we find the left-hand side to be 0.09, and the criterion seems well satisfied.

Finally, for the sake of consistency, we also checked our original assumption regarding growing waves. Substituting all of the relevant parameters into Eq. (3.8), we find that the left-hand side is of the order of 0.01, fulfilling the inequality.

B. Enhanced bremsstrahlung measurement

1. *Description*

Since the estimate of the energy enhancement factor $a\simeq 10^3$ is rather dependent upon the theoretical "plasmon model" of the previous sections, another independent diagnostic test was required. Of the various plasma turbulence effects, the enhanced bremsstrahlung radiation[55,56] at the plasma frequency ω_p and its harmonic $2\omega_p$, due to the interaction of longitudinal electron waves with plasma inhomogeneities and with themselves, respectively, can serve as a probe of the fluctuating electric field and the enhancement factor a.

For the measurement of this radiation a mesh filter combination, basically one reflecting filter plus one transmitting filter, was carefully chosen to get suitable wavelength positions and adequate bandwidths. A commercially made InSb detector was used. The signal-to-noise ratio was optimized by a bias current $I_d=300$ μA and a supplemental magnetic field $B=11$ kG. This corresponds to an effective crystal resistance $R_c=10$–15 kΩ, and after combining with the stray capacitance $C_s=30$–50 pF the detector shows some integration with a time constant in the region of 1 μsec.

The plasma density varies from 8×10^{13} to 4×10^{14} cm^{-3}; thus the $2\omega_p$ radiation could cover the wavelength region of ~ 0.8 to ~ 2.5 mm. Three combinations of mesh filters were made, centered at 1.00, 1.37, and 2.13 mm, with bandwidths 0.75, 0.96, and 1.31 mm, respectively, according to the transmittance calibration done by Advanced Kinetics, Inc. Finally, the detector was absolutely calibrated using the Osram mercury lamp, assuming a blackbody radiation at 3000 °K. (This assumption is quite good in the present wavelength region, where the fused-quartz envelope is transparent.[57])

2. *Estimate of enhanced bremsstrahlung radiation (at $2\omega_p$)*

A theoretical estimate of the enhanced bremsstrahlung at ω_p and $2\omega_p$ in a turbulent plasma, based on a fluid model, was first made by Sturrock *et al.*[27] Following their derivation, we obtain the total power emitted at $2\omega_p$ (which is believed due to plasmon-plasmon head-on collisions):

$$J_{\text{turb}}=\sqrt{3}\,\frac{8\pi^2}{5}\frac{e^2\omega_p^2}{m^2c^5}\times\int_0^\infty 4\pi k^2\,dk\,U^2(k)\ \text{erg sec}^{-1}\,\text{cm}^{-3}\,\text{sr}^{-1}, \tag{4.10}$$

where $U(k)$ is the total energy associated with a single longitudinal mode in some volume V and wave-number interval $k, k+dk$. $U(k)$ can also be expressed

$$\frac{U(k)}{V}\simeq\frac{1}{2}\frac{|\vec{E}_k|^2}{8\pi}\frac{\partial}{\partial\omega_k}(\omega_k\epsilon_L)\simeq\frac{|\vec{E}_k|^2}{8\pi}, \tag{4.11}$$

with ϵ_L being the longitudinal dielectric constant for electron oscillations. Equation (4.11) indicates that $U(k)$ is about twice the corresponding electric field energy, and from Eq. (3.11) we can write

$$U(k)\simeq A(\omega_k)\kappa T. \tag{4.12}$$

Combining Eqs. (3.12), (3.14), and (4.12), we can rewrite Eq. (4.10) as

$$J_{\text{turb}}=Fa^2\int_{\omega_p}^\infty\frac{\exp\{-[(\omega_k-\omega_0)/\Delta\omega]^2\}}{\omega_k(\omega_k^2-\omega_p^2)^{1/2}}d\omega_k, \tag{4.13}$$

where

$$F=\frac{16\pi^2}{15}\frac{e^2\omega_p^6}{c^5}\left(\frac{\kappa T}{m}\right)^{1/2}.$$

Predictions from the equivalent Lorentzian model are ~ 20% lower, since the square of the energy U_k is larger by a factor $4/\pi$ and the bandwidth smaller by a factor $\sim\sqrt{2}$.

3. *Transition layer*

Because of the large scale of the plasma column (nearly 3 m long along the optical axis), radiative transfer must be considered. It is dominated by inverse bremsstrahlung. The corresponding absorption coefficient, after allowing for stimulated emission, can be expressed

$$\kappa_\nu=3.692\times10^8(1-e^{-h\nu/\kappa T})\,g\,T_e^{-1/2}\,\nu^{-3}N_eN_i\ \text{cm}^{-1}, \tag{4.14}$$

where g is the usual Gaunt factor, which is of the order of unity for this experiment. Applying the Rayleigh-Jeans approximation, i.e., $h\nu\ll\kappa T$, we have

$$\kappa_\nu=1.98\times10^{-23}\lambda^2T_e^{-3/2}N_eN_i\,g\ \text{cm}^{-1}, \tag{4.15}$$

where T_e is given in °K. With $N_i = N_e = 3 \times 10^{14}$ cm^{-3}, $T_e = 0.7$ eV, and by using the criteria of Oster[58] to get $g \simeq 2.7$, the effective absorption coefficient for the continuum radiation at $2\omega_{pe}$ is estimated to be 0.1 cm^{-1}.

In principle, the plasma collective effect can enhance not only the bremsstrahlung emission but also the absorption. For instance, the photon may decay into plasmons and eventually be absorbed through Landau damping. We evaluate this absorption coefficient $\bar{\kappa}$ from the fluid model of Sturrock *et al.*,[27]

$$\bar{\kappa} \simeq \frac{8\pi}{3^{3/2}c}\left(\frac{e}{m\omega_p^2}\right)^2 \sum_{\vec{k}} (-\gamma_k)\, k^2\, \frac{|\vec{E}_k|^2}{8\pi}. \qquad (4.16)$$

By changing

$$\sum_{\vec{k}} \rightarrow V \int \frac{4\pi k^2\, dk}{(2\pi)^3}$$

and substituting the first-order Landau damping rate for γ_k,

$$\gamma_k \simeq -\left(\frac{\pi}{8}\right)^{1/2} \frac{\omega_p}{k^3\rho_D^3} \exp\left[-\left(\frac{3}{2} + \frac{1}{2k^2\rho_D^2}\right)\right], \qquad (4.17)$$

Eq. (4.16) can be simplified to

$$\bar{\kappa} \simeq 0.2\, W_{el}/\tfrac{3}{2}\, NKT = 0.2\xi \approx 0.005 \text{ cm}^{-1}, \qquad (4.18)$$

which is negligibly small in comparison with the inverse bremsstrahlung coefficient.

To the first order of approximation, we divide the plasma into two layers: the one inside the coil (layer 1) with turbulent plasma, and the one outside the coil (layer 2), with thermal plasma only. By denoting $N_e^{(2)} = \alpha N_e^{(1)}$, $T_e^{(2)} = \beta T_e^{(1)}$, with $0 \le \alpha \le 1$ and $0 \le \beta \le 1$, and assuming the bandwidth $\Delta\lambda$ of the mesh filter combination to be wide enough to cover the entire turbulent spectrum near $2\omega_{pe}$, we can obtain the integrated bremsstrahlung intensity. A choice of $\alpha = 0.9$–1.0, $\beta = 0.6$–0.7, was found quite reasonable and consistent with Balmer-line (total) intensities measured side on. It provided an enhancement factor a between 700 and 1000 (see Table III).

The measured bremsstrahlung is in general greater than the theoretical thermal level by a factor of $\gtrsim 10$ for the turbulent plasma and a factor of $\lesssim 4$ for the control plasma. All this further confirms that the n-α satellites we observed are indeed related to Langmuir turbulence and that the threshold condition (3.24) is not much exceeded.

4. *Discussion*

At the very instant of implosion, because of "antiparallel" polarities between the main discharge and the bias field, the existence of a "neutral layer" and therefore of "dual-energy" electrons seems plausible.[59] Dual energy simply means that a group of thermal electrons at temperature T_e coexists with a flux of suprathermal electrons at temperature χT_e, where χ could be as high as several orders of magnitude. This group of suprathermal electrons then drives the longitudinal fluctuation spectrum up to a high amplitude, probably via a process of Čerenkov

TABLE III. Bremsstrahlung measurements.

Filter band (mm)	$I(\nu)$ [a]	$B(\nu)$ [b]	α	β	a
Turbulent plasma: $N_e \simeq 3.14\times10^{14}$ cm^{-3}, $T_e \simeq 0.7$ eV, $2\omega_p \simeq 10.4$ cm^{-1} $\leftrightarrow \lambda \simeq 0.97$ mm					
1.0 ± 0.75	6.10×10^{-6}	6.70×10^{-7}	0.95	0.70	~930
1.4 ± 0.96	2.65×10^{-6}	3.40×10^{-7}	0.95	0.70	~1030
2.13 ± 1.3	1.22×10^{-6}	1.47×10^{-7}			
Turbulent plasma: $N_e \simeq 1.8\times10^{14}$ cm^{-3}, $T_e \simeq 0.5$ eV, $2\omega_p \simeq 8.1$ cm^{-1} $\leftrightarrow \lambda \simeq 1.25$ mm					
1.0 ± 0.75	5.18×10^{-6}	4.82×10^{-7}	1.0	0.60	~800
1.4 ± 0.96	2.19×10^{-6}	2.46×10^{-7}	1.0	0.60	~780
2.13 ± 1.3	0.86×10^{-6}	1.06×10^{-7}			
Control plasma: $N_e \simeq 1.4\times10^{14}$ cm^{-3}, $T_e \simeq 0.6$ eV, $2\omega_p \simeq 7.1$ cm^{-1} $\leftrightarrow \lambda \simeq 1.4$ mm					
1.0 ± 0.75	3.07×10^{-6}	5.78×10^{-7}			
1.4 ± 0.96	1.20×10^{-6}	2.94×10^{-7}	1.0	0.60	~330
2.13 ± 1.3	0.51×10^{-6}	1.27×10^{-7}			

[a] $I(\nu)$: measured bremsstrahlung.

[b] $B(\nu)$: theoretical thermal bremsstrahlung after optical depth correction, in units of W/(cm^2 sr cm^{-1}).

emission of electron plasma waves[60] or by some microinstability.[61] A possible explanation for the long duration of the turbulence lies in the continuing oscillations of the driving field (see Fig. 1). The resulting azimuthal electron drift velocity at our times of observation is estimated to be between the ion sound speed and the electron thermal speed. This rules out the two-stream instability as cause of the Langmuir wave excitation. However, the formation of a "neutral layer" may still imply the existence of suprathermal electrons.

An estimate of "threshold" turbulence for the generation of satellite peaks has been attempted by plotting $\zeta = I_{\text{satellite}} / I_{\text{unshifted}}$ for different $(\Delta\tilde{\nu}, a)$. It is then found that ζ is proportional to the product of $\Delta\tilde{\nu}$ and a in the region of interest; therefore no threshold enhancement factor can be deduced from our theoretical model. However, there is an experimental threshold due to the uncertainty in the continuum and the poor apparatus resolution. Setting a cutoff $\zeta \simeq 0.20$, we find that the satellites are not observable unless $a\Delta\nu > 30$. For the case of the turbulent plasma, where $\Delta\tilde{\nu} \simeq 0.085$, we have $a_{\text{threshold}}$ in the vicinity of 400. For the case of the control plasma, $\Delta\nu$ is expected to be smaller than 0.085; this implies $a_{\text{threshold}} > 400$, which is consistent with the result shown in the Table III. None of these conclusions are significantly changed if the assumed Gaussian plasma spectrum is replaced by a Lorentzian form, except that the (relative) width parameter is then $\Delta\tilde{\nu}' \approx 0.060$.

Finally, we would like to point out that the highest hydrogen n-α transition reported as observed in the laboratory prior to our work[26,41,42] appears to be the seventh transition $n = 8 \rightarrow 7$ at $\lambda = 19.06$ μm.[62]

V. CONCLUSIONS

Based on all the results presented in the preceding sections, the following conclusions may be drawn:

(1) The hydrogen n-α transitions (12-α at λ88.7 μm, 11-α at λ69.0 μm) exhibit satellite structures in a turbulent plasma; the displacement of the satellites is close to the electron plasma frequency ω_p, and hence interpreted as resulting from plasmon-atom collisions.

(2) Long-wavelength electric field fluctuations are found to be enhanced over a bandwidth of $\sim 0.1\ \omega_p$ by a factor $\gtrsim 10^3$ above the thermal level at $T_e \simeq 0.7$ eV, corresponding to a root-mean-square field strength $E \simeq 5.7$ kV/cm or an electrical energy $\sim 3\%$ of the electron thermal energy.

(3) Measurements of continuum radiation in the wavelength region near ω_p and $2\omega_p$ show significantly higher intensities than what would be expected for a thermal plasma; an enhancement factor of $\sim 10^3$ is also obtained from this method after radiative-transfer corrections are taken into consideration.

(4) The fluctuating field energy in the control plasma experiment is enhanced by merely a fac- of 300, which is consistent with the estimated experimental threshold $\simeq 400$ for the n-α satellites and the absence of satellites in this case.

ACKNOWLEDGMENTS

The authors gratefully acknowledge the advice and help of Dr. D. P. McNutt and Dr. W. J. Moore of the Naval Research Laboratory in building the infrared detector.

---

*Work supported by National Science Foundation.

†Present address: Laboratory for Laser Energetics, University of Rochester, Rochester, N. Y.

‡Some of the material in this paper is part of a Ph.D. thesis (see Ref. 41).

[1]H. R. Griem, *Spectral Line Broadening by Plasmas* (Academic, New York, 1974).

[2]J. Holtsmark, Ann. Phys. (Leipz.) 58, 577 (1919).

[3]M. Baranger, Phys. Rev. 111, 481 (1958); 111, 494 (1958); 112, 855 (1958).

[4]A. C. Kolb and H. R. Griem, Phys. Rev. 111, 514 (1958); H. R. Griem, A. C. Kolb, and K. Y. Shen, *ibid.* 116, 4 (1959).

[5]D. G. Yakovlev, Zh. Tekh. Fiz. 42, 1557 (1972) [Sov. Phys.-Tech. Phys. 17, 1248 (1973)].

[6]H. R. Griem, in *Advances in Atomic and Molecular Physics*, edited by D. R. Bates (Academic, New York, 1975), Vol. 11.

[7]T. M. O'Neil, Phys. Fluids 17, 2247 (1974).

[8]G. V. Sholin and E. A. Oks, Dokl. Adad. Nauk SSSR 209, 1318 (1973) [Sov. Phys.-Doklady 18, 254 (1973)].

[9]N. Ben-Yosef and A. G. Rubin, Phys. Lett. 33A, 222 (1970).

[10]E. K. Zavoiskii, Yu. G. Kalinin, V. A. Skoryupin, V. V. Shapkin, and G. V. Sholin, Dokl. Akad. Nauk SSSR 194, 55 (1970) [Sov. Phys.-Doklady 15, 823 (1970)].

[11]L. P. Zakatov, A. G. Plakhov, V. V. Shapkin, and G. V. Sholin, Dokl. Akad. Nauk. SSSR 198, 1306 (1971) [Sov. Phys.-Doklady 16, 451 (1971)].

[12]A. S. Antonov, O. A. Zinov'ev, V. D. Rusanov, and A. V. Titov, Zh. Eksp. Teor. Fiz. 58, 1567 (1970) [Sov. Phys.-JETP 31, 838 (1970).

[13]S. P. Zagorodnikov, G. E. Smolkin, E. A. Striganova, and G. V. Sholin, Zh. Eksp. Teor. Fiz. Pis'ma Red. 11, 475 (1970) [JETP Lett. 11, 323 (1970)].

[14]S. P. Zagorodnikov, G. E. Smolkin, E. A. Striganova, and G. V. Sholin, Dokl. Akad. Nauk 195, 1065 (1971) [Sov. Phys.-Doklady 15, 1122 (1970)].

[15]A. B. Berezin, L. B. Dubovoi, B. V. Lublin, and D. G. Yakovlev, Zh. Tekh. Fiz. 42, 946 (1972) [Sov. Phys.

Tech. Phys. 17, 750 (1972)].
[16]H. R. Griem and H. J. Kunze, Phys. Rev. Lett. 23, 1279 (1969).
[17]W. R. Rutgers and H. deKluiver, Z. Naturforsch. A 29, 42 (1974); W. R. Rutgers and H. W. Kalfsbeek, *ibid.* 30, 739 (1975).
[18]C. Gallagher and M. Levine, Phys. Rev. Lett. 30, 897 (1973); C. Gallagher and M. Levine, J. Quant. Spectrosc. Radiat. Transfer 15, 275 (1975).
[19]T. J. Nee and H. R. Griem, Bull. Am. Phys. Soc. 20, 605 (1975).
[20]M. Baranger and B. Mozer, Phys. Rev. 123, 25 (1961).
[21]D. Blochinzew, Phys. Z. Sowjetunion 4, 501 (1933); E. V. Lifshitz, Zh. Eksp. Teor. Fiz. 53, 943 (1967) [Sov. Phys.-JETP 26, 570 (1968)].
[22]A. Cohn, P. Bakshi, and G. Kalman, Phys. Rev. Lett. 29, 324 (1972); P. Bakshi, G. Kalman, and A. Cohn, *ibid.* 31, 1576 (1973).
[23]W. W. Hicks, Lawrence Radiation Laboratory Report No. LBL-2470, 1974 (unpublished).
[24]V. N. Tsytovich, *Nonlinear Effects in Plasma* (Plenum, New York, 1970).
[25]R. C. Davidson, *Methods in Nonlinear Plasma Theory* (Academic, New York, 1972).
[26]T. R. LaSalle, T. J. Nee, and H. R. Griem, Phys. Rev. Lett. 30, 944 (1973).
[27]P. A. Sturrock, R. H. Ball, and D. E. Baldwin, Phys. Fluids 8, 1509 (1965).
[28]D. Williamson, J. Opt. Soc. Am. 42, 712 (1952).
[29]A. Hadni, J. Claudel, G. Morlet, and P. Strimer, Appl. Opt. 1, 161 (1968).
[30]A. Hadni, *Essentials of Modern Physics Applied to the Study of the Infrared* (Pergamon, New York, 1967).
[31]R. Kaplan, Appl. Opt. 6, 685 (1967).
[32]E. H. Putley, Phys. Status Solidi 6, 571 (1964).
[33]P. D. Feldman and D. P. McNutt, Appl. Opt. 8, 2205 (1969).
[34]W. J. Moore, U. S. Naval Research Laboratory Report No. 1493, 1965 (unpublished).
[35]W. J. Moore and H. Shenker, Infrared Phys. 5, 99 (1965).
[36]*The Art and Science of Growing Crystals*, edited by J. J. Gilman (Wiley, New York, 1963), p. 327.
[37]W. J. Moore (private communication).
[38]RCA Semiconductor Data Book, File No. 218 (unpublished).
[39]R. Green, Rev. Sci. Instrum. 39, 1495 (1968).
[40]R. R. Wagner, P. T. Anderson, and B. Bertman, Rev. Sci. Instrum. 41, 917 (1970).
[41]T.-J. Nee, Ph.D. thesis, Tech. Report No. 76-033 (University of Maryland, 1975) (unpublished).
[42]T. R. LaSalle, Ph.D. thesis, Tech. Report No. 73-079 (University of Maryland, 1972) (unpublished).
[43]*Spectroscopic Techniques*, edited by D. H Martin (North-Holland, Amsterdam, 1967).
[44]A. J. Lichtenberg and S. Sesnic, J. Opt. Soc. Am. 56, 75 (1966).
[45]E. W. Smith, J. Cooper, and C. R. Vidal, Phys. Rev. 185, 140 (1969); D. Voslamber, Z. Naturforsch. A 24, 1458 (1969).
[46]M. Abramowitz and I. A. Stegun, *Handbook of Mathematical Functions*, U. S. Natl. Bur. Stand. Appl. Math. Series 55 (U.S. GPO, Washington, D.C., 1964).
[47]P. M. Morse and H. Feshbach, *Methods of Theoretical Physics* (McGraw-Hill, New York, 1953).
[48]R. B. White, Y. C. Lee, and K. Nishikawa, Phys. Rev. Lett. 29, 1315 (1972).
[49]V. E. Zakharov, Zh. Eksp. Teor. Fiz. 62, 1745 (1972) [Sov. Phys.-JETP 35, 908 (1972)].
[50]K. Nishikawa, Y. C. Lee, and C. S. Liu (unpublished).
[51]S. Ichimaru, *Basic Principles of Plasma Physics, a Statistical Approach* (Benjamin, Reading, Mass., 1973).
[52]H. R. Griem, Astrophys. J. 148, 547 (1967).
[53]G. Peach, Astrophys. Lett. 10, 129 (1972).
[54]H. Capes and D. Voslamber, Phys. Rev. A 5, 2528 (1972).
[55]C. Chin-Fatt and H. R. Griem, Phys. Rev. Lett. 25, 1644 (1970); C. Chin-Fatt, Phys. Fluids 17, 1410 (1974).
[56]R. S. Post and T. C. Marshall, Phys. Fluids 17, 452 (1974).
[57]G. Rogoff and S. Brown, Rev. Sci. Instrum. 41, 1500 (1970).
[58]L. Oster, Rev. Mod. Phys. 33, 525 (1961).
[59]N. L. Bretz, Ph.D. thesis, Tech. Report No. 73-073 (University of Maryland, 1972) (unpublished).
[60]D. A. Tidman and T. H. Dupree, Phys. Fluids 8, 1860 (1965).
[61]V. B. Krasoviikii, Zh. Eksp. Teor. Fiz. 66, 154 (1974) [Sov. Phys.-JETP 39, 71 (1974)].
[62]P. Hansen and J. Strong, Appl. Opt. 12, 429 (1973).